Impact of In-plane Perforations on Near-Wellbore Fracture Geometry in Horizontal Wells

Feng Sun, Shifeng Xue
China University of Petroleum (East China), Qing Dao, Shan Dong, China
Meirong Tang, Xiang Zhang, Bing Ma
Oil and Gas Technology Research Institute of Changqing Oilfield Branch Company, Xi'an, Shaan Xi, China

ABSTRACT:

Perforations provide the fluid conduit between the wellbore and the formation. In-plane perforation is a new perforating strategy for unconventional reservoir hydraulic fracture stimulation, with parameters change such as gun phasing, orientation and spacing that impact the outcomes in the near wellbore region. To address the impact of in-plane perforations on near-wellbore fracture geometry, a 3D coupled hydro-mechanical finite element model is developed, together with a continuum-based damage mechanics constitutive approach. Damage variable governs the deterioration of stiffness with strain, and the damage affects the crack element modeling that is used to consider crack behavior and to construct a crack-tracking algorithm that simulated propagation. Using field data from Changqing Oilfield, series of sensitivities have been performed to quantify the impact of different perforation schemes on fracture-initiation pressure, rupture location and fracture geometry. The results indicate that the stress interference between the perforations is increased for horizontal well with in-plane perforation, which can reduce the fracture initiation pressure 2.0-3.5MPa. The in-plane perforations guide the initial fracture trajectory extend towards the preferred fracture plane, and transverse fractures are created. It would avoid the tortuous near-wellbore fracture geometry and beneficial to wellbore-to-fracture connectivity.

1. INTRODUCTION

Perforations play an important role in determining the near-wellbore fracture geometry during the stimulation phase. The choice of perforation parameters, such as shot density, shot phasing, interval length, and gun orientation, has a significant effect on the geometry of the hydraulic fracture (Behrmann and Nolte 1999; Waters and Weng 2016). Optimized perforation numbers and location lead to significant improvements in well performance (Lecampion et al. 2015).

The fracture tortuosity in near wellbore of the horizontal well is undesirable, as they increase the average treating pressure and potentially impact the wellbore-to-fracture connectivity during production. The in-plane perforation technique (Liu et al. 2014) was proposed to change conventional spiral distribution of firing holes and adopt special charge distribution mode for horizontal wells (Fig. 1). The intention of in-plane perforation is to form multi-perforation tunnel towards a fan-shaped plane (preferred fracture plane), which perpendicular to the axial of the horizontal well, and can effectively control the trend of the initial fracture and reduce breakdown pressure.

Gaining a better understanding of fracture initiation and propagation from perforations is essential for efficient hydraulic fracture treatment. Numerical approaches have been applied to analyze the complicated stress-state of the perforated wellbore and the fracture-initiation process. The finite element method (FEM) was employed to analyze the impact of perforations on fracture geometry in horizontal wells (Busetti et al. 2012; Sun, Jia, and Xue 2019). The boundary element method (BEM) was employed to investigate the problem of fracture initiation and perforation failure, and 3D models were built to evaluate the fracture-initiation pressure and to predict the location and direction of the initial crack (Alekseenko et al. 2012).

For the impact of in-plane perforation, experimental testing program in a large-scale apparatus was undertaken to verify its effect on reduce breakdown pressure and improve near-wellbore fracture geometry (Falser et al. 2016). The mechanism of fracture initiation and the influence rules of in-plane perforating parameters on the fracture initiation pressure were analyzed with FEM method (Liu et al. 2015). The above researches have mainly focused on predicting the location and direction of initial crack. They rarely provide information on effect of

perforation parameters on fracture propagation and coalescence among multiple perforations. In addition, they simplified the spatial positions of all in-plane perforations holes into a cross-section plane, while the influence of the perforation holes incline angle is ignored.

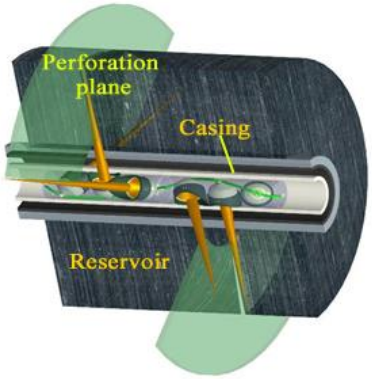

Fig. 1. Schematic diagram of in-plane perforation (Liu et al. 2014)

In this study, the impact of in-plane perforations on fracture geometry in horizontal wells is addressed through use of a three-dimensional coupled stress-pore pressure finite element model, together with a continuum-based damage mechanics (CDM) constitutive approach. Complex fracture geometry due to damage (initiation, propagation and coalescence of fractures) in the 3D problem statement is presented. The CDM model allows the exploration of the range of orientations and perforation parameters most suitable for the in-plane perforating completions that are used for hydraulic fracture stimulation.

2. COUPLED HYDRO-MECHANICAL MODEL

To address the coupled process of hydraulic fracturing in near-well region of horizontal well, i.e., the interaction between fluid flow and deformation (fracture), coupled hydro-mechanical model is developed (Xu and Wong 2013; Yin, Dusseault, and Rothenburg 2007).

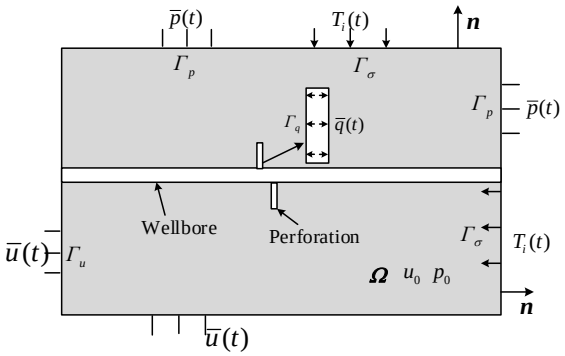

Fig. 2. Schematic of the problem domain

Consider a porous continuum in the domain Ω and the bounded by surface Γ , as illustrate in Fig. 2. The governing equation for the equilibrium of porous media with fluid saturated in domain Ω can be expressed as:

$$\sigma_{ij,j} + f_i = \sigma'_{ij,j} - \alpha p_{,i} + f_i = 0 \tag{1}$$

Combined with the constitutive relationship of Hooke's law, the elastic deformation equation of rock could be obtained as:

$$Gu_{i,jj} + \frac{G}{1-2\nu} u_{j,ji} - \alpha p_{,i} + f_i = 0 \tag{2}$$

where, σ_{ij} is the stress tensor, σ'_{ij} is the effective stress tensor, tension is taken as positive, f_i is the body force in solid skeleton, α is the Biot coefficient, p is pore pressure, u is displacement, G is shear modulus, ν is Poisson's ratio.

The mass balance equation of fluid flow in deformable porous media is written as:

$$\phi C_f \frac{\partial p}{\partial t} - \frac{k}{\mu}\nabla^2 p + \alpha \frac{\partial e}{\partial t} = Q \tag{3}$$

According to Darcy's law for fluid flow, the flow rate q is described as:

$$q = -\frac{k}{\mu}(\nabla p + \rho_f g \nabla Z) \tag{4}$$

where, ϕ is the porosity , C_f is fluid compressibility, e is the volumetric strain of rock mass, Q is the source-sink term of the seepage process, k is rock permeability, μ is fluid viscosity, ρ_f is fluid density, and Z is elevation.

The initial conditions and boundary conditions are stated below:

(i) Initial conditions

$$u_i(0) = u_0, \quad p(0) = p_0 \quad \text{in } \Omega \tag{5}$$

(ii) Boundary conditions

$$\begin{cases} u_i = \bar{u}(t) & \text{on } \Gamma_u \\ \sigma_{ij} \cdot n_j = T_i(t) & \text{on } \Gamma_\sigma \\ p = \bar{p}(t) & \text{on } \Gamma_p \\ -\dfrac{k}{\mu}\nabla p = \bar{q}(t) & \text{on } \Gamma_q \end{cases} \tag{6}$$

where, u_0 , p_0 are the displacement and pressure of initial domain, $\bar{u}(t)$, $\bar{p}(t)$ are the displacement and pressure of boundary, $T_i(t)$ is the boundary force, n_j is the cosine of exterior normal direction, $\bar{q}(t)$ is the fluid flux, Γ_u , Γ_σ , Γ_p , and Γ_q are the bound surface of the displacement, stress, pore pressure and flux, respectively.

3. CONTINUUM DAMAGE EVOLUTION MODEL

Continuous damage mechanics identify materials with locally discrete micro-flaws (micro-cracks and micro-holes) as continuum models, and describe the materials damage process with damage variables(Sarvaramini, Dusseault, and Gracie 2018; Shojaei, Dahi Taleghani, and Li 2014).

Focusing on the mechanism of fracture growth from perforation to near-wellbore in horizontal wells, continuum-based damage elements was defined to characterize the three-dimensional fracture rupture position and geometry evolution. Two stress-state parameters, e.g. tensile state variable and compressive state variable, were used to describe the continuous damage around the perforation and near-wellbore region.

For tensile state (at least one of the principal stresses is tensile), the damage variable is defined as:

$$D=\begin{cases}0 & \varepsilon_t<\varepsilon_{t0}\\ 1-\dfrac{f_{tr}}{E_0\varepsilon_t} & \varepsilon_t\ge\varepsilon_{t0}\end{cases} \tag{7}$$

The damage variable under compressive state (all three principal stresses are compressive) can be expressed as:

$$D=\begin{cases}0 & \varepsilon_c>\varepsilon_{c0}\\ 1-\dfrac{f_{cr}}{E_0\varepsilon_c} & \varepsilon_c\le\varepsilon_{c0}\end{cases} \tag{8}$$

The equivalent strain is calculated as:

$$\begin{cases}\varepsilon_t=\sqrt{\sum_{i=1}^{3}\left(\dfrac{|\varepsilon_i|+\varepsilon_i}{2}\right)^2}\\ \varepsilon_c=\min(\varepsilon_1,\varepsilon_2,\varepsilon_3)\end{cases} \tag{9}$$

where, D is the damage variable, ε_t , ε_c are the equivalent principal strain for tensile and compressive state, ε_{t0} , ε_{c0} are the elastic limit of tensile and compressive strain, ε_i (i =1,2,3) are the three principal strains, f_{tr} , f_{cr} are the residual tensile and compressive strength.

In continuum damage mechanics (CDM), damage can be considered as a macroscopic state variable that affects stiffness degradation of the material, and used to modify the stiffness matrix for a failure element (Lee and Ghassemi 2011; Tang et al. 2002).

The stress distribution, hydraulic fracture initiation and propagation of perforation tips and near wellbore and is analyzed, based on the failure element concept. Information on failure element, time, and position are recorded in a dataset at each time step. Based on the damage mechanics theory, the Young's modulus of the element degrade gradually during damage progresses and the damage evolution law of the damaged element is defined as follows:

$$E=(1-D)E_0 \tag{10}$$

where, E and E_0 represent the Young's moduli of the damaged elements and undamaged elements.

The elastic deformation equation (2) for the damaged skeletal material which exhibits isotropic damage can be expressed in following form:

$$G(1-D)u_{i,jj}+\frac{G(1-D)}{1-2\nu}u_{j,ji}-\alpha p_{,i}+f_i=0 \tag{11}$$

Because of the damage, permeability is correlated to damage effect within the failure elements. The permeability can be described as(Tang et al. 2002):

$$k=\xi k_0\exp(-\eta\bar{\sigma}') \quad 0<D\le 1 \tag{12}$$

where, k_0 is the initial permeability, η is a coupling coefficient, $\bar{\sigma}'$ is the effective average stress, ξ is the mutation coefficient, which reflects the permeability mutation in the damage element.

4. FINITE ELEMENT FORMULATION

By applying the Green-Gauss theorem and Galerkin weighted residual method, the rock matrix continuum deformation-damage Eq. (11) and the continuity equation for fluid flow (3) can be converted into the matrix form after finite element discretization:

$$\begin{cases}[\mathbf{K}]\mathbf{u}+[\mathbf{Q}]\mathbf{p}=\mathbf{f}^u\\ [\mathbf{S}]\dot{\mathbf{p}}+[\mathbf{H}]\mathbf{p}+\left[\mathbf{Q}^{\mathrm{T}}\right]\dot{\mathbf{u}}=\mathbf{f}^q\end{cases} \tag{13}$$

where, $\mathbf{u}$, $\mathbf{p}$ are the vectors of displacement and pressure, and $\dot{\mathbf{u}}$, $\dot{\mathbf{p}}$ are corresponding time derivatives. The matrix expressions are listed as follows.

$$\mathbf{K}=\int_\Omega \mathbf{B}^{\mathrm{T}}\mathbf{D}\mathbf{B}d\Omega \quad \mathbf{Q}=\int_\Omega \alpha\mathbf{B}^{\mathrm{T}}\mathbf{m}\mathbf{N}_p d\Omega \tag{14}$$

$$\mathbf{S}=\int_\Omega \mathbf{N}_p^{\mathrm{T}}\phi C_f\mathbf{N}_p d\Omega \quad \mathbf{H}=\int_\Omega \nabla\mathbf{N}_p^{\mathrm{T}}\frac{k}{u}\nabla\mathbf{N}_p d\Omega \tag{15}$$

$$\mathbf{f}^u=\int_\Omega \mathbf{N}_u^{\mathrm{T}}\mathbf{f}d\Omega+\int_{\Gamma_\sigma}\mathbf{N}_u^{\mathrm{T}}\mathbf{T}d\Gamma \quad \mathbf{f}^q=\int_{\Gamma_q^e}\text{-}\mathbf{N}_p^{\mathrm{T}}\bar{q}d\Gamma \tag{16}$$

To integrate equation with respect to time, the linear interpolation in time can be discretized with standard finite difference methods, and the incremental forms of the above FE equations can be written as:

$$\begin{cases}[\mathbf{K}]\mathbf{u}_{t+\triangle t}=[\mathbf{K}]\mathbf{u}_t+[\mathbf{Q}]\Delta\mathbf{p}_t+\triangle\mathbf{f}^u\\ [\mathbf{S}+\theta\Delta t\mathbf{H}]\mathbf{p}_{t+\triangle t}=\left[\mathbf{S}-(1-\theta)\Delta t\mathbf{H}\right]\mathbf{p}_t-\left[\mathbf{Q}^{\mathrm{T}}\right]\Delta\mathbf{u}_t+\Delta t\mathbf{f}^q\end{cases} \tag{17}$$

where, $\mathbf{u}_{t+\Delta t}$, $\mathbf{p}_{t+\Delta t}$ represent the solution at the current time step, $\mathbf{u}_t$, $\mathbf{p}_t$ is the solution at last time step, θ is an integration parameter in the interval $0 \le \theta \le 1$.

The displacement convergence criterion is used to judge the convergence of incremental solution

$$\Delta\varepsilon = \sum_{i=1}^{node} \frac{\Delta u_t^2}{u_t^2} \le 10^{-5} \tag{18}$$

where, $\Delta\varepsilon$ is the iterative tolerance of the displacement increment, $\Delta u_t = u_{t+\Delta t} - u_t$ is the displacement increment at current time step, u_t is the displacement at last time step.

An incremental finite element procedure is developed using the continuum damage evolution criteria, and the iterative decoupling method is used to solve the above equations of geomechanics and reservoir flow variables.

Given a set of initial values, the fluid pressure, the displacement, strain and stress are computed from Eq. (17) from updated and boundary conditions. The coupling iteration is controlled by a convergence criterion which is based on Eq. (18). The stress concentration region gradually reach the fracture initiation criterion, this region's elements are defined as damage elements. And the damage elements' matrices **K** and **H** are determined using Eq. (7), (8) and (12).

In this way, the initiation and growth of fracture can be described using continuum damage mechanics.

5. NUMERICAL EXAMPLE SETUP

Numerical simulations have been performed to analyze the effects of in-plane perforation parameters on initial fracture location and near-wellbore fracture complexity of horizontal well. Field data from Changqing Oilfield (Xi'an, China) is introduced to perform the numerical simulation analysis.

5.1. Model configuration

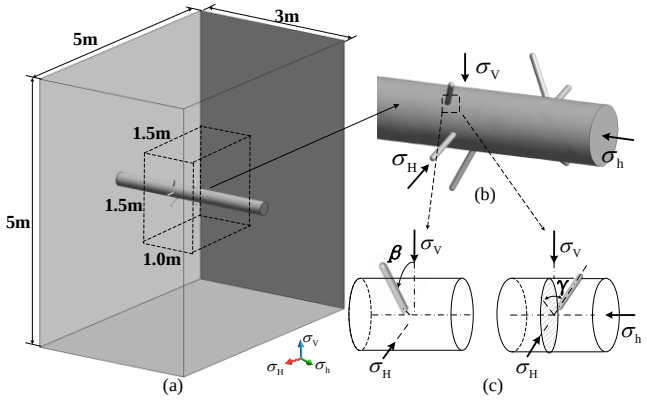

Fig.3 Computational geometry models (a) Model geometry; (b) In-plane perforation model; (c) In-plane perforation angle parameters.

The wellbore is assumed to be located at the center of a block, and the near wellbore block of 1.0 m×1.5 m×1.5 m is selected to local encryption of element mesh. The model has one perforation cluster, which includes 6 perforation tunnels, and the phase angle of perforation tunnels is 60°. We assume the direction of two middle perforations is consistent with the maximum horizontal stress σ_H. The perforation tunnel length is 400mm, and the diameter of perforation tunnel is 20mm.

According to field data, the Young's modulus of reservoir is 21.5 GPa, Possion's ratio is 0.23, shear modulus is 8.75 GPa, tensile strength is 3.0 MPa, cohesion strength is 6.0 MPa, porosity is 8.92%, and permeability is 1.0×10^{-3}μm^2. Parameters used for CDM models are listed in Table 1.

Table 1. Reservoir properties and well parameters

Parameters	Symbols	Values
Residual tensile strength	f_{tr}	0.45 MPa
Residual compressive strength	f_{cr}	0.9 MPa
Mutation coefficient	ξ	10.0
Coupling coefficient	η	0.025

The applied far-field in-situ stresses: vertical stress σ_v =43.0 MPa, maximum horizontal stress σ_H =38.0 MPa, and minimum horizontal stress σ_h =34.0 MPa are applied on three sides, as shown in Fig. 3. The other three sides of the model is applied as roller boundary conditions. For fluid phase, the pore pressure of the reservoir p =18.0MPa is applied as the initial condition. No-flow boundary condition is applied on all sides. As displays in Fig.3 (c), β is the deflection angle of perforation tunnel relative to the vertical direction, and γ is the incline angle of perforation tunnel with wellbore cross section.

5.2. Model validation

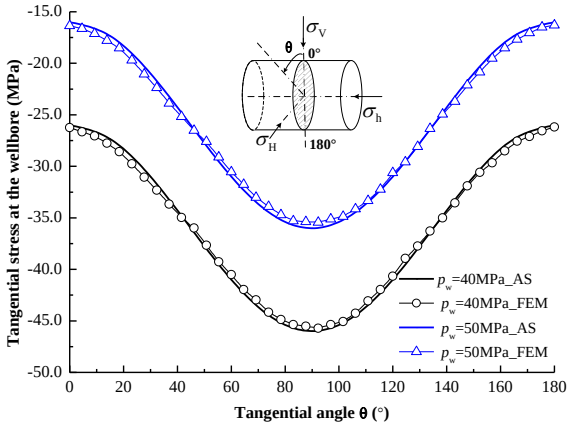

Fig. 4 Tangential stress distribution along the open-hole horizontal wellbore

The FEM model was validated against the results of analytical model and perforation fracture experiments.

The tangential stress distribution along the open-hole horizontal wellbore is shown as Fig. 4. We compare the FEM results with Hossain's analytical solution (Hossain, Rahman, and Rahman 2000), and there's a difference of less than 3.5%.

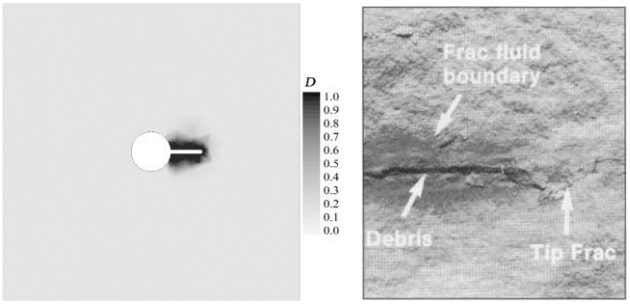

(a) Simulation result (b) Experimental image

Fig.5 Comparison of damage fracture geometry of perforation

Fig. 5 compares the damage fracture geometry between numerical simulation results and that of the perforation fracture experiments(Behrmann and Elbel 1991). One can see a good agreement of the damage zone along the perforation between them. The above results show that the developed FEM model can be used to analyze the stress and fracture geometry in the near-well region.

6. RESULTS AND DISCUSSIONS

6.1. Sensitivity of fracture initiation to perforation direction

The effect of perforation direction on initial fracture geometry is analyzed through various perforation deflection angle β and perforation incline angle γ.

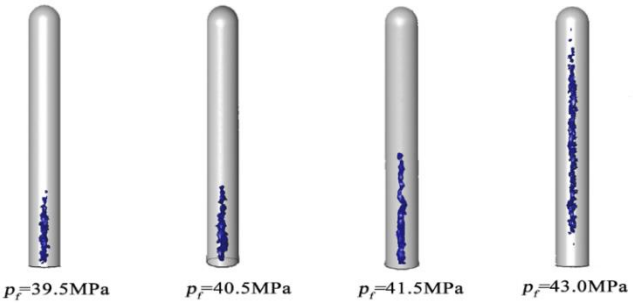

(a) β=0° (b) β=30° (c) β=60° (d) β=90°

Fig. 6 Initial fracture geometry for different perforation deflection angle β

The effect of perforation orientation on initial fracture geometry is analyzed through various angle β relative to the vertical direction. For cased-cement horizontal well, the initiated fractures are all transverse to the wellbore (Fig.6). For $\beta \leq 60°$, fractures initiate from the perforation base. While β continues increasing, the initial fracture position is extended from base to the middle and tip of the tunnel.

According to the numerical results, it is obvious that the initiation of the fractures is sensitive to perforation orientation. With the increase of the perforation deflection angle β, the fracture initiation pressure p_f grows up to its maximum at β=90°, the p_f difference between various perforation angles are 3.5MPa.

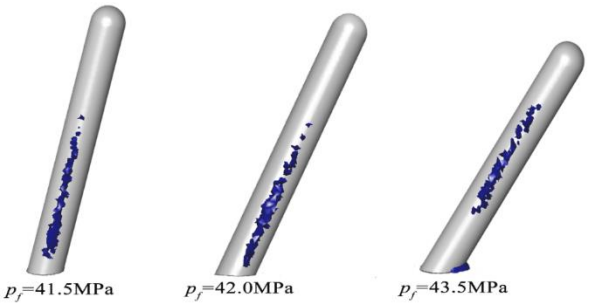

(a) γ=15° (b) γ=25° (c) γ=35°

Fig. 7 Initial fracture geometry for different perforation incline angle γ

The in-plane perforation changes the direction of jet flow by adjusting the incline angle γ of perforation bullet. We investigate the influence of the incline angle γ on the initial fracture geometry and p_f with fixed angle β=30°. As shown in Fig. 7, two possible scenarios of fracture initiation are observed. With the comparatively small angle (γ=15°, γ=25°), the zones for rock failure located along perforation axis. However, the fracture scenarios would be initiating from the remote side of the perforation channel and the wellbore/perforation interface similarly for γ=35°cases.

6.2. Impact of perforation parameters on initial fracture geometry of horizontal well

Based on continuum damage mechanics, the failure elements' matrices of stiffness and seepage are modified. The post-failure and growth of fracture can be described by the damage-driven crack element modeling. Fig.8 present the initial fracture geometry of horizontal well with different perforation scheme.

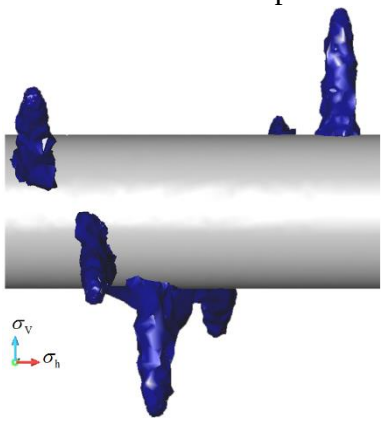

(a) Case-cement horizontal well with spiral perforation

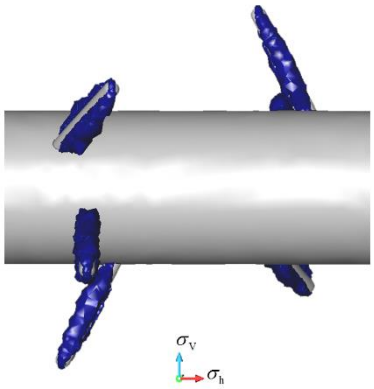

(b) Case-cement horizontal well with in-plane perforation (γ=25°)

Fig. 8 Comparison of initial fracture geometry of horizontal well perforating

The stress interference between the spiral perforation channels control the direction of fracture propagation in local region of perforation. With the pressure increase, the damaged zone extends and links-up among multi-perforations, as shown in Fig. 8(a).

By adjusting the tunnel inclined angle γ, in-plane perforation can control the initial fracture directions of the perforation. As shown in Fig. 8(b), the fracture of side perforations initiates and extends along the perforation axis, leading to the coalescence of fractures.

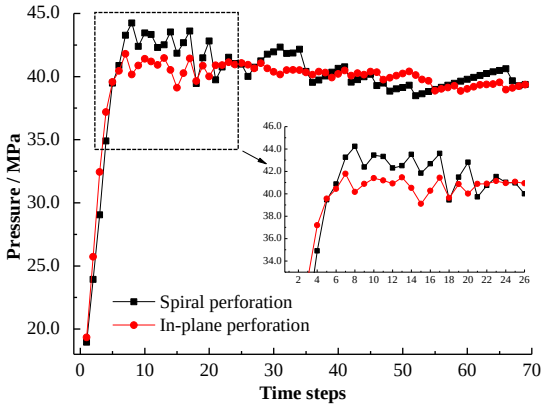

Fig. 9 Comparison of pressure change with different perforation strategy

Fig. 9 presents the comparison of fracture pressure for two kinds of perforation strategies. For horizontal well with spiral perforation, the fracture initiation pressure is 44.5 MPa The field fracturing pressure recording of this well 43.0MPa.

Due to the stress interference between multiple holes, the fracture initiation pressure of in-plane perforation is reduced to 41.3 MPa. This value is 3.2 MPa lower than the conventional spiral perforation case. The field fracturing pressure is 39.3 MPa, which is in a good agreement with the simulation data.

Fig.9 displays that the initial fracture propagation pressure of spiral perforation is 2.0~3.0 MPa higher than in-plane perforation. This differences is due to the effect of perforation on near-wellbore fracture geometry.

6.3. Fracture geometry for in-plane perforations of horizontal well

The in-plane perforation technique designs perforation axis aiming at the preferred fracture plane, and the stress interference of multi-perforations increases. By adjusting the tunnel inclined angle γ, in-plane perforation can control the initial fracture directions of the perforation.

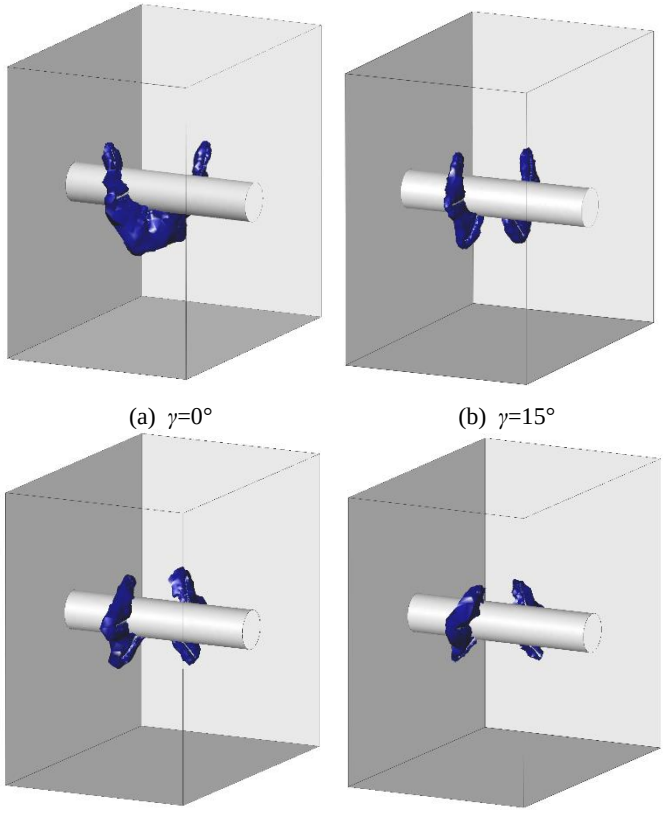

(a) γ=0° (b) γ=15°

(c) γ=25° (d) γ=35°

Fig. 10 Fracture geometry of near-wellbore for different incline angle γ

Fig. 10 depicts the damage evolution process around the wellbore for different perforation parameters. For γ=0°, i.e. spiral perforation, fracture extends through each perforation as they spiral around the casing and form the fracture geometry with spiral distortion. The near-wellbore tortuosity causes additional friction and pressure drops. It's not conductive to initiate transverse fractures at the near wellbore, and impact the wellbore-to-fracture connectivity of horizontal wellbore.

For in-plane perforation (Fig. 10b, 10c, 10d), the crack extends along the inclined perforation and deflects to the damage zones of the middle tunnels. Two preferred fan shaped plane, perpendicular to the axial of the casing, are

formed. For γ=35°, the near wellbore fracture morphology appears to be two sets of fractures oblique to the horizontal wellbore axis. Thus, within the range of perforation incline angle $\gamma \leq 25°$, the in-plane perforations guide the initial fracture trajectory towards the preferred fracture plane, and transverse fractures are created. It would avoid the tortuous near-wellbore fracture geometry and is beneficial to wellbore-to-fracture connectivity.

7. CONCLUSIONS

A coupled hydro-mechanical finite element program is developed and employed to analyze the impact of perforations on fracture geometry in horizontal wells. Within the framework of continuum mechanics, the scalar damage variable is used to represent stiffness degradation and damage-drive fracturing model is used to investigate the propagation of near wellbore fracture geometry.

The sensitivity study performed revealed that perforation can be used to control the fracturing pressure and the initial fracture position with the variation of angle between the direction of the perforation channel and the preferred fracture plane. A complex and tortuous near-well fracture geometry tends to be induced in conventional spiral perforations. With optimized direction of jet flow of the in-plane perforation, the initial fracture trajectory can be directed towards the preferred fracture plane, and the tortuosity of near-wellbore fracture can be reduced. This will improve the efficiency of hydraulic fracturing stimulation.

ACKNOWLEDGEMENTS

This research was supported by the National Natural Science Foundation of China (No. 51304230), and the Fundamental Research Funds for the Central Universities (16CX05001A).

REFERENCES

1. Alekseenko, O. P., D. I. Potapenko, S. G. Cherny, D. Esipov, D. Kuranakov, and V. Lapin, 2012, 3-D Modeling of Fracture Initiation From Perforated Non-Cemented Wellbore. *SPE Hydraulic Fracturing Technology Conference* 18(03):589–600.
2. Behrmann, L. A., and J. L. Elbel, 1991, Effect of Perforations on Fracture Initiation. *JPT*, 43(May):608–15.
3. Behrmann, L. a., and K. G. Nolte, 1999, Perforating Requirements for Fracture Stimulations. *SPE Drilling & Completion* 14(4):18–19.
4. Busetti, S., K. Mish, P. Hennings, and Z. Reches, 2012, Damage and plastic deformation of reservoir rocks: Part 2. propagation of a hydraulic fracture. *AAPG Bulletin* 96(9):1711–32.
5. Falser, S., and W. Mo, 2016, Reducing breakdown pressure and fracture tortuosity by in-plane perforations and cyclic pressure ramping. *50th US Rock Mechanics / Geomechanics Symposium*.
6. Hossain, M., M. Rahman, and S. Rahman, 2000, Hydraulic fracture initiation and propagation: roles of wellbore trajectory, perforation and stress regimes. *Journal of Petroleum Science and Engineering* 27(3–4):129–49.
7. Lecampion, B., J. Desroches, X. Weng, J. Burghardt, and J. E. Brown, 2015, Can We Engineer Better Multistage Horizontal Completions? Evidence of the Importance of Near-Wellbore Fracture Geometry From Theory, Lab and Field Experiment. in *SPE Hydraulic Fracturing Technology Conference*. Society of Petroleum Engineers.
8. Lee, S. H., and A. Ghassemi, 2011, Three-Dimensional Thermo-Poro-Mechanical Modeling Of Reservoir Stimulation And Induced Microseismicity In Geothermal Reservoir. *Thirty-Sixth Workshop on Geothermal Reservoir Engineering, 31 January-3 February*.
9. Liu, H., F. Wang, Y. Wang, Y. Gao, and J. Cheng, 2014, Oil well perforation technology: Status and prospects. *Petroleum Exploration and Development* 41(6):798–804.
10. Sarvaramini, E., M. B. Dusseault, and R. Gracie. 2018. Characterizing the Stimulated Reservoir Volume During Hydraulic Fracturing-Connecting the Pressure Fall-Off Phase to the Geomechanics of Fracturing. *Journal of Applied Mechanics* 85(10): 101006.
11. Shojaei, A., A. Dahi Taleghani, and G. Li, 2014, A continuum damage failure model for hydraulic fracturing of porous rocks. *International Journal of Plasticity* 59: 199–212.
12. Sun, F., P. Jia, and S. Xue, 2019, Continuum Damage Modeling of Hydraulic Fracture from Perforations in Horizontal Wells. *Mathematical Problems in Engineering* 2019:1–12.
13. Tang, C. A., L. G. Tham, P. K. K. Lee, T. H. Yang, and L. C. Li, 2002, Coupled analysis of flow, stress and damage (FSD) in rock failure. *International Journal of Rock Mechanics and Mining Sciences* 39(4):477–89.
14. Waters, G., and X. Weng, 2016, The Impact of Geomechanics and Perforations on Hydraulic Fracture Initiation and Complexity in Horizontal Well Completions. in *SPE Annual Technical Conference and Exhibition*. Society of Petroleum Engineers.
15. Xu, B., and R. C. K. Wong, 2013, Coupled finite-element simulation of injection well testing in unconsolidated oil sands reservoir. *International Journal for Numerical and Analytical Methods in Geomechanics* 37(18):3131–49.
16. Yin, S., M. B. Dusseault, and L. Rothenburg, 2007, Coupled multiphase poroelastic analysis of reservoir depletion including surrounding strata. *International Journal of Rock Mechanics and Mining Sciences* 44(5):758–66.